EPJ manuscript No.
(will be inserted by the editor)

One- and two-component colloidal glasses under transient shear

T. Sentjabrskaja[1,a], M. Laurati[1,2], and S.U. Egelhaaf[1,b]

[1] Condensed Matter Physics Laboratory, Heinrich Heine University, 40225 Düsseldorf, Germany
[2] División de Ciencias e Ingenierías, Universidad de Guanajuato, 37150 León, Mexico

Abstract. In concentrated colloidal mixtures different caging mechanisms exist and result in different arrested states: repulsive, attractive and asymmetric glasses as well as gel-like states. We discuss their microscopic structure, dynamics and rheological response. Special attention is given to the non-linear mechanical behaviour, in particular the transient rheological response after shear is started. Steps in both, shear rate and shear stress (creep test), are considered. The macroscopic viscoelastic response is related to the microscopic structure and dynamics on the individual-particle level.

1 Introduction

Many particle dispersions used in applications, for example paint or cement, and also dispersions occurring in nature, for example clays, are characterised by size distributions of the dispersed phase. The distribution might be continuous, i.e. polydisperse, or discrete, in the simplest case containing only two distinct species. It is often difficult to avoid a distribution of particle sizes and hence to prepare a monodisperse system. Then again, through the presence of several species the properties of a dispersion, such as its phase behaviour and mechanical properties, can be tuned, for instance to meet processing or application needs.

The size distribution affects many features, for example crystallization [1–9] and the glass transition [10–29], but also mechanical and other properties. Here we focus on the glass transition and the mechanical properties of glasses. One-component dispersions of hard-sphere colloids have frequently been used as model systems to study the glass transition [28,29]. In this system, the volume fraction ϕ is the only control parameter. For volume fractions beyond $\phi_g \approx 0.58$ (and a sufficiently broad size distribution) dynamical arrest with the absence of long-distance diffusion has been found [24,27–33]. Arrest is driven by crowding. Particles are trapped in cages formed by their neighbours, at least until activated processes may restore long-time diffusion [34].

Addition of a second species significantly affects the dynamics and can melt one-component glasses [25–27,35–39]. Such mixing effects strongly depend on the size

[a] present address: Department of Systems Biophysics, AMOLF, Amsterdam, the Netherlands
[b] e-mail: stefan.egelhaaf@uni-duesseldorf.de

ratio δ and the composition. At small to moderate size disparities (up to about 1:3), the glass transition shifts to larger total volume fractions as compared to the one-component system, similar to the effect of polydispersity [11,25,12,27,40] or the behaviour at random close packing (RCP) where the presence of different species allows for more efficient packing [41–48]. For large size disparities (beyond 1:5), four qualitatively different glasses have been predicted by mode-coupling theory (MCT) [26, 27,24] and self-consistent generalized Langevin equation theory (SCGLE) [12]. The arrested states differ by the caging mechanisms and include repulsive, attractive and asymmetric glasses as well as gel-like structures. The transitions between the arrested states (except between the repulsive and attractive glasses) involve fluids. Some of these states were observed experimentally [25,13] and in simulations [14,15]. However, the experimental evidence was limited to the observation of the onset of dynamical arrest. Only recently the different arrested states were quantitatively characterized in terms of their microscopic structure and dynamics on the single-particle level [16–18, 49].

The rheological properties, in particular the solid-like behaviour, correlate with dynamical arrest. The linear viscoelastic moduli reflect the formation and melting of the different glass states [16–18]. Upon glass formation, the viscoelastic properties are characterized by a sharp increase of the viscosity and the appearance of a Maxwell plateau modulus in the linear response [50–65]. Similarly, the melting of a glass is reflected in a strongly reduced viscosity but also faster particle dynamics [11,50,66, 67].

Shear can induce the melting and flow of arrested states [68–83]. Shear-induced melting is associated with structural changes, e.g. an irreversible deformation of the cage [73,77,81,82], and dynamical changes, e.g. the onset of diffusive dynamics [72], and involves yielding [68–71,83]. The transient regime during which these changes occur will be discussed in the following. Particular emphasis will be given to the link between the macroscopic rheological response and the transient structure and dynamics on the individual-particle level. The experimental investigation of these issues benefits from recent technical advances, namely in confocal microscopy and its combination with rheology [84,85] as well as in quantitative data analysis methods [84,86]. We focus on binary mixtures of hard-sphere-like particles [17,87,88], namely sterically-stabilized polymethylmethacrylate (PMMA) spheres [28,89]. Binary mixtures are the simplest multi-component system but nevertheless allow for the investigation of different arrested states and fluids in a single model system. Thus, they are an ideal colloidal model system. Furthermore, the results might also be relevant for other glassy materials, including polymers [90] and metallic alloys [91].

2 Quiescent State – Structure and Dynamics

Binary mixtures are characterized by the size ratio $\delta = R_\mathrm{S}/R_\mathrm{L}$, where R_S and R_L are the radii of the small and large particles, respectively, their total volume fraction ϕ and their composition, here quantified by the fraction of small particles, $x_\mathrm{s} = \phi_\mathrm{s}/\phi$, where ϕ_s is the volume fraction of small particles. First, we consider samples with a constant total volume fraction $\phi \approx 0.60$ and a small size ratio $\delta \approx 0.09$, which results in the largest number of arrested states when the fraction of small spheres, x_s, is varied: repulsive, attractive and asymmetric glasses [26] as well as a gel-like structure (Fig. 1). The transitions between the arrested states involve fluid states, except between repulsive and attractive glasses. In all arrested states at least the large particles are arrested. In the following hence particular emphasis is given to the dynamics of the large particles.

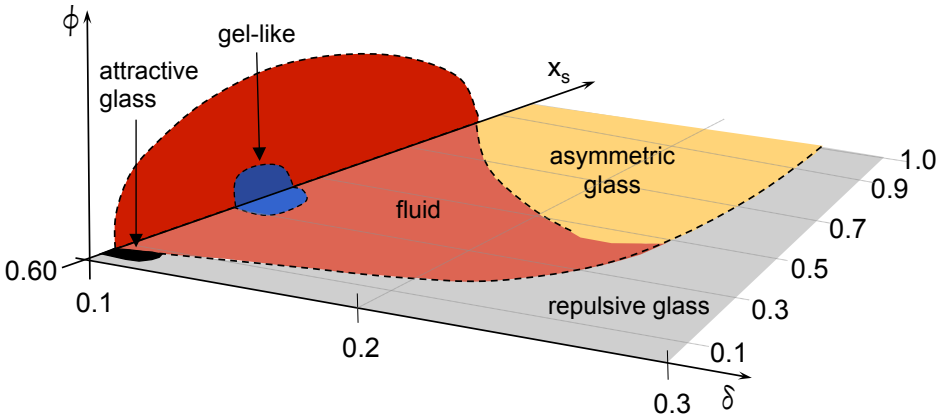

Fig. 1. Schematic state diagram as a function of size ratio δ, total volume fraction ϕ and fraction of small particles, x_s. Depending on these parameters, different states are observed: repulsive (grey) and attractive glasses (black), gel-like structures (blue), asymmetric glasses (yellow) and fluids (red).

The one-component samples ($x_s = 0.0$ and 1.0) are repulsive glasses showing the characteristic arrested dynamics with a localization on a length scale of about 10% of the particle diameter [28,29,92,93]. If a small amount of small spheres is added ($x_s \approx 0.01$), the large particles experience depletion-induced attractions and an attractive glass is formed [26,12], similar to the one observed in colloid-polymer mixtures [94–98]. They exhibit an extended plateau in the mean squared displacement (MSD) of the large spheres with a slightly smaller localization length and hence a tighter cage than in the one-component systems [49]. The tightening is attributed to attractions induced by the small particles rather than their intercalation between the large particles. The attractions also lead to a space-spanning network of large particles with a small correlation length and hence a quite homogenous distribution of the very dense large particles.

At this composition, the small particles are mobile within the network of large particles. This resembles the classical Lorentz gas [99–101] with the main difference that the large particles are not immobile but very slow. In the classical Lorentz gas, the motion of the small particles becomes localized when the large particles percolate and thus the voids are disconnected. In the present situation, however, the voids regain connections on the slow time scale of the rearrangements of the large particles. Thus the dynamics of the small particles is controlled by percolation, leading to localization, as well as glassy dynamics, leading to *transient* localization. This interplay leads to anomalous transport of the small particles above a critical size ratio, $\delta_c \approx 0.35$. For length scales comparable to the size of the large particles, the density autocorrelation function as well as the collective and self density fluctuations do not show the power-law decay predicted for the classical Lorentz gas close to the percolation transition, but a logarithmic decay that extends over at least three decades in time [102].

If the fraction of small particles is increased beyond $x_s \approx 0.01$, the amount of large particles becomes too small to form a glass. Furthermore, the small particles can very efficiently pack in the voids between the large particles. The pair distribution function $g(r)$ indeed indicates that small particles are located between the large particles [16–18]. Due to the efficient packing and the intercalation of small spheres, the remaining cages of the large particles are distorted, loosened and increasingly delocalized. This results in faster dynamics of the large particles. The glass melts and a fluid phase forms.

For intermediate $x_s \approx 0.3$, due to the increasing amount of small particles the depletion-induced attractions between the large particles become strong enough to induce a gel with many particle contacts and a significant structural heterogeneity [26,24,49,103]. This leads to an arrest of the large particles. Their localisation length is considerably smaller than in the repulsive and attractive glasses, but the plateau and subdiffusion are less pronounced. Similar gels are found in other systems [104–113].

If the gel-structure is diluted by adding further small particles, the system-spanning network becomes fluid-like and both particle species mobile. The large particles show an especially enhanced dynamics where they are in contact with the more mobile small particles [114,115].

Once the amount of small spheres is large enough ($x_s \approx 0.9$) they become arrested. Moreover, they form a dense matrix in which the large particles are embedded and are also arrested. An asymmetric or *torroncino* glass has formed [26,49]. Due to the ability of the small particles to tightly pack around the large particles, the cages are smaller than cages formed by large spheres, even by large spheres in the presence of attractions. Correspondingly, the dynamics exhibit the smallest localization length, an extended plateau and the most pronounced dynamical arrest. Asymmetric glasses were also reported in binary mixtures of size asymmetric star polymers [116,117] and are most likely present in binary mixtures of silica particles [13].

As described above, the localization becomes stronger with increasing x_s, whereas the dynamical arrest shows a minimum at intermediate x_s. The arrest is particularly strong for $x_s \approx 0.9$ but also for small x_s, whereas it is less pronounced for the arrested gel structure at intermediate $x_s \approx 0.3$. This corresponds to the x_s dependence of the long-time structural relaxation time of the large particles which shows a minimum at intermediate x_s (in contrast to the long-time structural relaxation time of the small particles which monotonously increases) [18]. It furthermore coincides with a maximum in the available free volume assuming that this follows the x_s dependence of the volume fraction of random close packing [16–18,41,43–47]. The asymmetry of the minimum is also attributed to the fact that the addition of small particles melts the glass of large particles whereas the addition of large particles not only melts the glass of small particles but also introduces obstacles [118]. Due to the different x_s dependences of the long-time structural relaxation times of the large and small particles, their structural relaxation times dominate at small and large x_s, respectively [18]. Accordingly, a transition in the arrest mechanism from caging by large to caging by small particles occurs at intermediate x_s [17].

When the particle species become more similar, i.e. δ closer to unity, a smaller number of arrested states is found [16–18]. Upon an increase to $\delta = 0.2$, the repulsive and possibly an attractive glass as well as an asymmetric glass are formed but no evidence for a gel state has been reported yet [16–18]. For larger size ratios ($\delta \gtrsim 0.4$) only a repulsive glass state is observed [17]. Finally, for $\delta \gtrsim 0.67$ small particles were found to no longer intercalate between the large particles [119], in agreement with geometrical arguments suggesting a similar limiting size ratio $\delta \approx 0.41$ [17]. With increasing δ, furthermore, the difference in the dynamics of the arrested and fluid states becomes smaller [11,25,17,19,21,40].

3 Transient Response – Rheology, Structure and Dynamics

The composition of binary mixtures affects their rheological response. It influences the linear and non-linear response in oscillatory shear experiments, including the flow curve [16,17,120,121], as well as the transient responses after shear is switched on or

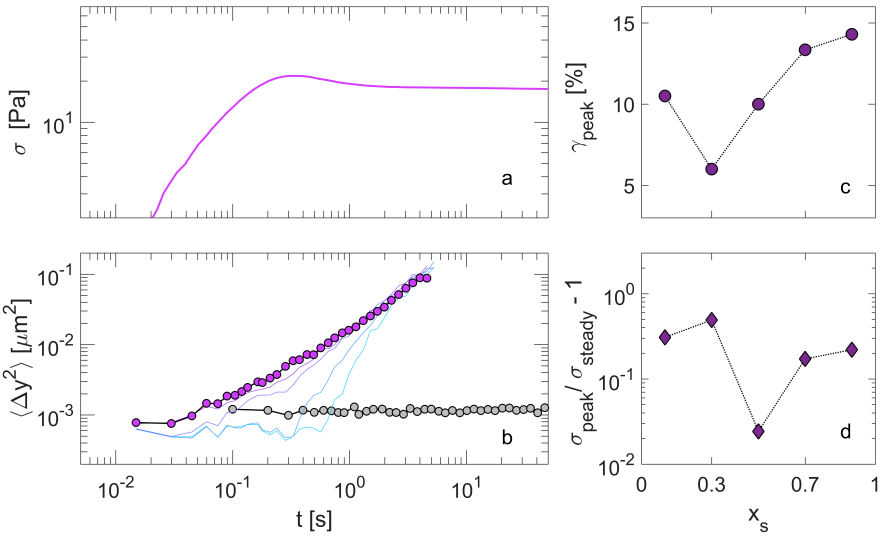

Fig. 2. Evolution of (a) the stress σ (shear rate $\dot{\gamma} = 0.348$ s^{-1}) and (b) the mean squared displacement (MSD) $\langle \Delta y^2 \rangle$ ($\dot{\gamma} = 0.147$ s^{-1}) after application of the shear rate as a function of time $t = \gamma/\dot{\gamma}$. The MSD in the quiescent state (●), after different waiting times (lines, increasing from right to left) and once the steady-state is reached (●) are shown. The dependences of (c) the location, $\gamma_{\rm peak}$, and (d) the magnitude, $\sigma_{\rm peak}/\sigma_{\rm steady} - 1$, of the overshoot as a function of the fraction of small particles, $x_{\rm s}$. Sample with a size ratio $\delta = 0.2$, total volume fraction $\phi = 0.61$ and fraction of small particles $x_{\rm s} = 0.9$.

off [81,122]. In the following we concentrate on the transient response after shear is switched on.

3.1 Step in shear rate

In a step rate experiment, a constant shear rate $\dot{\gamma}$ is applied to the initially quiescent sample and the evolution of the stress σ as a function of time t or, equivalently, strain $\gamma = \dot{\gamma}\, t$ is measured (Fig. 2a) [16,18,51,72,73,77,78,82,123–126]. The stress initially increases linearly and then deviates from linear behaviour to reach a maximum. The overshoot or maximum stress, $\sigma_{\rm peak}$, is reached at the strain $\gamma_{\rm peak}$, typically $\gamma_{\rm peak} \approx 10\%$. Upon adding small particles, $\gamma_{\rm peak}$ decreases, reaches a minimum at $x_{\rm s} \approx 0.3$ and then increases again (Fig. 2c), which reflects the distance to the glass transition; $\gamma_{\rm peak}$ is larger for systems deeper in the glass [18]. The strain $\gamma_{\rm peak}$ has been associated with the yield strain [73,77,82]. After the overshoot, the stress decreases and reaches a steady state of flow with a constant stress value, $\sigma_{\rm steady}$. The magnitude of the stress overshoot, $\sigma_{\rm peak}/\sigma_{\rm steady} - 1$, characterizes the ability to store and release stress. As a function of $x_{\rm s}$, the magnitude of the overshoot also shows an intermediate minimum which, however, occurs at $x_{\rm s} \approx 0.5$ (Fig. 2d) [18]. The minimum has been associated with the maximum cage compressibility which also occurs for this value of $x_{\rm s}$ and the release of stored stress in this process. This stress response, in particular the stress overshoot, has been observed in colloidal glasses [16,18,72,73,77,123–125] as well as other systems [127–132]. In experiments with metallic glasses, the overshoot typically is observed at comparable strains if the different shear protocols, namely uniaxial compression instead of shear strain, are taken into account. The rheological response has successfully been described by mode coupling theory (MCT) [78,123,

133]. Furthermore, a phenomenological theory has linked the microscopic nearest neighbour rearrangements to the macroscopic stress response [83].

The quiescent particle structure and dynamics not only influence the rheological response but, at the same time, the applied shear also modifies the particle arrangement and dynamics with respect to the quiescent state. Shear increasingly deforms the cage (where the cage might be formed by the large and/or small particles depending on x_s) [73,82]. Accordingly, the MSD exhibits stronger, but now transient, localization than in the quiescent state (Fig. 2b). With waiting time, the transient localization is moderately reduced but remains stronger than in the quiescent state, reflecting the continuing shear-induced deformation of the cage. Moreover, superdiffusive dynamics is observed which progressively disappears with waiting time. Superdiffusion seems to pre-empt the overshoot [73,77,82,123,125]. The overshoot has been associated with the maximum sustainable deformation [73,77,78]. When this is reached, the cage breaks or yields. In the potential energy landscape picture, cage breaking has been associated with the crossing of energy barriers [127,134–139]. Once the cage is broken, the stress stored during cage distortion can partially be released and the cage deformation to some extent relaxed by out-of-cage motions. Stress can also somewhat be released through cage compression. This leads to the decrease in stress following the overshoot.

Eventually a steady-state of flow is reached with diffusive particle dynamics and some residual structural anisotropy [82,140,141]. The diffusion observed at long delay times [16,72,73,84,123–125,140,142] is reached earlier at longer waiting times as the superdiffusive regime progressively disappears [18] (Fig. 2b). The diffusion involves several particles and movements beyond the cage and hence has been linked to shear-induced cage break-up [140]. Accordingly, the long-time diffusion coefficient is dominated by the time scale imposed by shear and has been observed to scale as $\dot{\gamma}^{0.8}$ [72] and $\dot{\gamma}^{1}$ [143] in one-component glasses and much stronger dependences have been found in two-component glasses [18]. The diffusion coefficient shows a weak maximum at intermediate $x_s \approx 0.3$ which coincides with the fastest long-time dynamics in the quiescent state and the smallest γ_{peak} [18]. This suggests a link of the fast dynamics in the quiescent and steady-state with facilitated yielding, i.e. a small yield strain.

These findings indicate the importance of the interplay between the involved time scales. The structural relaxation time of the system diverges or might be limited by activated processes leading to diffusion at long times [34]. In any case, it is the longest time scale of the system. On the other hand, the Brownian time associated with the short-time diffusion of the large and small spheres is comparable to the time scale introduced by shear, $1/\dot{\gamma}$. Their relation is quantified by the Peclet number $Pe = 6\pi\eta\dot{\gamma}/\langle k_B T/R^3\rangle$ where η is the viscosity of the dispersion medium and $k_B T$ the thermal energy.

If the Peclet number Pe is small, i.e. if the shear-induced deformation is slow compared to the short-time Brownian dynamics, the peak position is approximately constant, $\gamma_{peak} \approx 10\%$ [78]. Thus the shear-induced cage deformation must be sufficiently large, $\gamma_{peak} \approx 10\%$ suggests about the cage size, that the initially caged particles can escape through Brownian motion in a cooperative manner. This then allows for the observed structural rearrangements, accelerated dynamics, yielding and glass melting. In contrast, for large Pe the peak position γ_{peak} increases [18,73,78,82, 125]. With increasing Pe, the particle displacements are increasingly dominated by shear-imposed affine motion whereas the contribution by Brownian motion decreases and becomes limiting. The increase of γ_{peak} with increasing Pe suggests that cage escape requires the particles to undergo Brownian motion for some time corresponding to a certain amount of particle collisions. Therefore, for yielding to occur cooperative movements are required with at least an affine displacement of about 10% as well as a minimum average Brownian displacement. The transition between the two regimes

occurs at $Pe \approx 1$ which suggests that it is determined by the interplay between the shear-induced time scale, $1/\dot{\gamma}$, and the short-time in-cage dynamics responsible for cage deformations. A similar dependence as for γ_{peak} was observed for the strain at which the steady state of flow is reached [144].

The magnitude of the overshoot, $\sigma_{\mathrm{peak}}/\sigma_{\mathrm{steady}}-1$, first increases and then decreases with increasing Pe [18,73,78,82,125]. This Pe dependence is similar to the ones of the superdiffusion and long-time diffusion coefficient. Thus the overshoot becomes more pronounced for faster dynamics, which also implies a higher probability of particle collisions. Moreover, the overshoot seems to increase as the localisation at rest becomes stronger. The transition between the two regimes depends on x_{s}. Since out-of-cage motions are involved, it is expected to depend on the structural relaxation time of the caging population in the quiescent state, i.e. the large particles for $x_{\mathrm{s}} \lesssim 0.3$ and the small particles for $x_{\mathrm{s}} > 0.3$ [16–18,73,82], which introduces an x_{s} dependence. Stress transmission involves particle movements on length scales of out-of-cage motions that are longer than those required for cage deformations, which determine γ_{peak}. Thus, the relations of the shear-induced time scale, $1/\dot{\gamma}$, with the time scales of the short-time and long-time dynamics, respectively, result in two different regimes of the Pe dependences of the yield strain γ_{peak} and the magnitude of the stress overshoot, $\sigma_{\mathrm{peak}}/\sigma_{\mathrm{steady}}-1$, as well as in different transitions between these regimes.

3.2 Step in shear stress (creep)

In a creep experiment, a step to a shear stress σ is applied and the induced deformation γ measured as a function of time (Fig. 3a) [51,71,91,107,126,145–160]. Different responses are possible. If the applied stress is comparable to the yield stress σ_{y}, i.e. $\sigma \approx \sigma_{\mathrm{y}}$, a characteristic creep response is observed with the strain increasing sublinearly with time, $\gamma \sim t^a$ with $a < 1$. For smaller $\sigma < \sigma_{\mathrm{y}}$, the deformation occurs extremely slowly and the system does not reach a steady state within the observation time. In contrast, if $\sigma \gg \sigma_{\mathrm{y}}$ a rapid transition to a steady-flow regime occurs, which implies $\gamma \sim t$. The scenario hence depends on the relation between σ and σ_{y}, where the latter depends on the size ratio δ, composition x_{s} and the total volume fraction ϕ. With decreasing δ, the minimum σ_{y} and hence the maximum softening becomes more pronounced and moves towards smaller x_{s} and thus the dependence becomes more asymmetric with respect to x_{s} [16–18].

The different regimes in the macroscopic strain response $\gamma(t)$ are reflected in the single-particle dynamics, namely $\langle \Delta y^2(t) \rangle$ (Fig. 3b). For $\sigma < \sigma_{\mathrm{y}}$, the extremely slow deformation is reflected in slow particle dynamics. At short times the MSD increases only slightly, indicating caging, whereas at long times subdiffusion occurs with $\langle \Delta y^2 \rangle \sim t^b$ with an exponent $b < 1$ which is very similar to the one of the rheological response, $b \approx a$. No significant dependence on waiting time is observed. Similar for $\sigma \approx \sigma_{\mathrm{y}}$, the macroscopic creep response without steady-state flow is reflected in subdiffusive particle dynamics. If $\sigma \gg \sigma_{\mathrm{y}}$, again caging occurs at short times but diffusion at long times with a transient superdiffusive regime at intermediate times that becomes shorter with waiting time and eventually disappears in the steady state of flow [81,124,140].

In steady flow, the MSD can be related to the strain; $\langle \Delta y^2(t) \rangle \sim D(\sigma)t \sim [D(\sigma)/\dot{\gamma}]\gamma(t) \sim \gamma(t)$ using for the diffusion coefficient $D \sim \dot{\gamma}^{0.8}$ or $D \sim \dot{\gamma}^1$ [72,142, 143]. This relation was implicitly assumed in a recent theoretical approach [161–163]. As expected, this relation is observed in steady-state flow ($\gamma \gg 10$). However, it was found to also hold in the transient regime prior to steady flow and even in the creep regime [158]. It is not observed only at very short times or, equivalently, very small

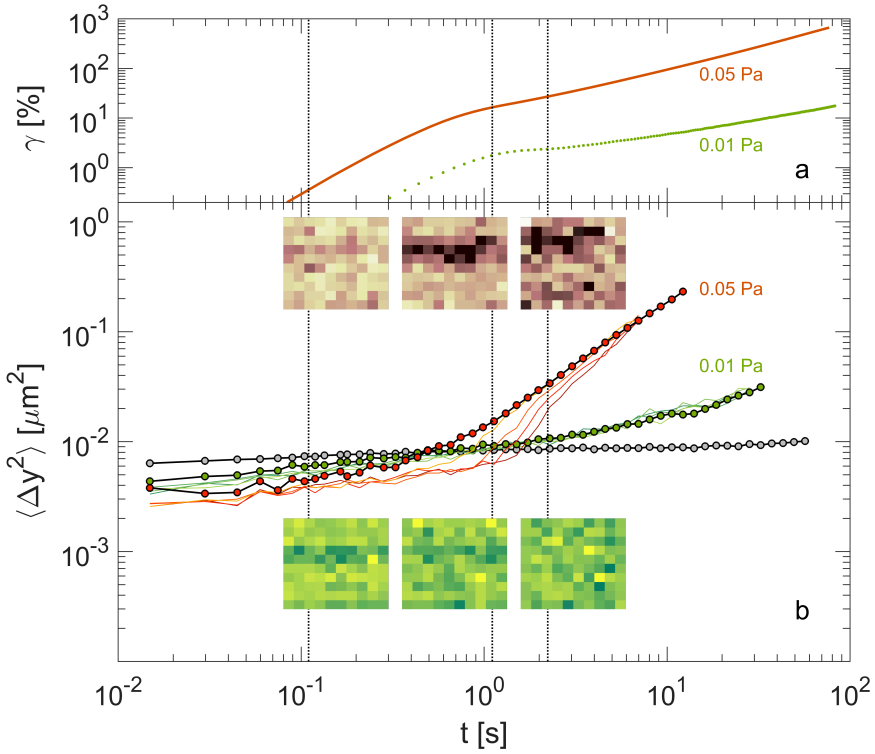

Fig. 3. Evolution of (a) the strain γ and (b) the mean squared displacement (MSD) $\langle \Delta y^2 \rangle$ after application of a stress of about the yield stress ($\sigma = 0.01$ Pa $\approx 1\sigma_y$; •) and above the yield stress (0.05 Pa $\approx 5\sigma_y$; •) as a function of time t. The MSD in the quiescent state (•), after different waiting times (lines, increasing from right to left) and once the steady-state is reached (symbols) are shown. The insets show the average local particle mobilities (indicated by the colour scale where dark colours correspond to high mobilities) as a function of time t (left to right, as indicated by dashed lines) for (bottom) $\sigma \approx 1\sigma_y$ and (top) $\sigma \approx 5\sigma_y$. The box size is $53\,\mu\text{m}^2$. Sample with $\delta = 0.2$, $\phi = 0.61$ and $x_s = 0.1$.

strains, i.e. in the initial elastic regime, as well as for short times and large stresses, which is attributed to the time lag between the particles' out-of-cage motions and the onset of macroscopic deformation. The relation between the MSD and the strain hence seems to be a consequence of the plasticity that develops after the initial elastic regime.

The single-particle dynamics can also be characterized by the distribution of displacements, the van Hove function $p(\Delta x)$. Its tails reveal that a small number of very mobile particles exists during the transient regime. The evolution of the fraction of mobile particles closely follows that of the strain $\gamma(t)$. Instead of individual particles, particles located in boxes, i.e. groups of particles, have been considered and a group defined active if their average particle mobility satisfies the same criterion as used in the case of the van Hove function (Fig. 3b, insets). Then, essentially independent of the size of the box or group, the fraction of active groups is found to grow as the fraction of individual active particles and hence also as $\gamma(t)$, which is proportional to $\langle \Delta y^2(t) \rangle$. This indicates that the mobile particles significantly contribute to $\langle \Delta y^2(t) \rangle$. This is observed for all stresses σ, i.e. below and above σ_y. A similar connection be-

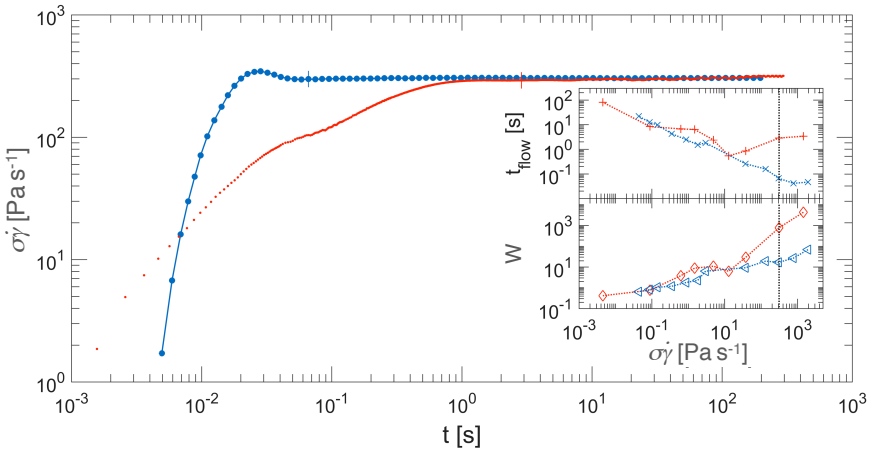

Fig. 4. Evolution of the power density $\sigma\dot{\gamma}$ as a function of time t after application of a step to a shear rate $\dot{\gamma} = 10.2$ s^{-1} (•) and to a stress $\sigma = 30.0$ Pa (•), respectively, where the values of $\dot{\gamma}$ and σ are chosen to result in a similar steady-state. (top inset) Time, t_{flow}, and (bottom inset) work per volume, W, required to reach the steady state of flow as a function of $\sigma\dot{\gamma}$ following both protocols (colours as in main figure). Sample with $\delta = 0.2$, $\phi = 0.61$ and $x_{\mathrm{s}} = 0.7$.

tween the number of active regions and γ was reported for frictional granular particles [164].

The existence of active particles and active groups of particles implies that the dynamics is heterogeneous. For $\sigma \approx \sigma_{\mathrm{y}}$, active regions exist but they do not grow and their locations vary randomly with time (Fig. 3b, lower inset). This is consistent with the subdiffusive particle dynamics. Similar mobilities occur for $\sigma > \sigma_{\mathrm{y}}$ at short times, i.e. when the localisation plateau in the MSD is observed. However, once superdiffusion occurs, regions with an enhanced mobility emerge, grow and span almost the whole sample once the system flows, where the characteristic length of the active regions increases with about $t^{2/3}$ (Fig. 3b, upper inset). The enhanced local mobilities occur through the accumulation of only slightly above-average local, non-affine particle displacements and do not result from sudden large displacements, as proposed in other systems [165–171]. Therefore, the onset of flow not only coincides with the appearance of superdiffusive dynamics but also extended active regions and pronounced non-Gaussian tails in the van Hove function. Once steady flow has developed, these features disappear and the dynamics again becomes more homogeneous.

3.3 Comparison of steps in shear rate and shear stress

Both protocols, a step to a strain rate and to a stress, result in a comparable steady-state of flow if the corresponding strain rate and stress, as given by the flow curve, are chosen (Fig. 4) [51,126,144]. However, a time scale is imposed if a shear rate is applied, whereas this is not the case in creep tests. In creep experiments, furthermore, regimes below yielding can be accessed. Thus the choice of control parameter determines the path from the quiescent state to the steady-state of flow. For example and as explained above, in creep experiments the MSD is proportional to the strain, $\langle \Delta y^2(t) \rangle \sim \gamma$, which has no analogue in the strain-controlled case where $\gamma(t)$ increases linearly with time but $\langle \Delta y^2(t) \rangle$ increases superlinearly in the transient regime. This indicates qualitative differences in the transient response to stress and strain-controlled shear.

To allow for a comparison of the transient regimes, the data are represented in a joint graph as the power density, i.e. the product $\sigma\dot{\gamma}(t)$ (Fig. 4) [144]. At long times, the steady state of flow is identical. In the transient regime, however, the responses differ and hence different paths are followed towards the steady state. For the step-rate experiment, $\sigma\dot{\gamma}(t)$ resembles $\sigma(t)$ (Fig. 2a) since $\dot{\gamma}$ is constant. Initially it steeply increases, reaches the overshoot and decreases to a constant value. In the creep experiment the increase of $\sigma\dot{\gamma}$ is more gradual and hence steady flow is achieved later. The time required to reach the steady state of flow, t_{flow}, monotonically decreases with increasing $\sigma\dot{\gamma}$ in step-rate experiments (Fig. 4, inset). In creep experiments, it initially also decrease but then increases again with $\sigma\dot{\gamma}$. The decrease for small $\sigma\dot{\gamma}$ is similar for both protocols. Due to the concomitant increase of $\dot{\gamma}$, flow begins at about the same strain independent of $\sigma\dot{\gamma}$. In contrast, for large $\sigma\dot{\gamma}$ steady flow is reached considerably later by application of constant stress. Similarly, also yielding is induced faster under constant shear rate than constant stress [144]. Furthermore, the composition, i.e. the glass state and caging mechanism, affects yielding in step-rate experiments whereas it seems not in creep experiments [144]. This might be due to the slower yielding process in creep experiments, in which the cage deforms intermittently rather than continuously. This might conceal the effects of the different caging mechanisms.

Also the efficiency to achieve yielding or to induce flow has been considered [144]. The work per volume, W, required to reach yielding or the steady state of flow is given by $W = \int \sigma\dot{\gamma}(t)\mathrm{d}t$ where the integral ranges from the application of shear until yielding or flow is reached. It depends on the time-dependent power density, $\sigma\dot{\gamma}(t)$, but also the time required to achieve yielding or flow. Less work is required if a step rate is applied which is due to the shorter time required to reach yielding and flow. The work increases with increasing $\sigma\dot{\gamma}$ indicating that yielding and flow is most efficiently, although slowly, achieved by applying a small stress (beyond the yield stress) or strain rate. At large $\sigma\dot{\gamma}$, the work increases about linearly with $\sigma\dot{\gamma}$ for all compositions x_{s} with the limiting behaviour occurring already at smaller $\sigma\dot{\gamma}$ for weaker glasses. In this regime, fluidization is reached quickly. This suggests that, beyond a minimum stress or shear rate, flow is induced almost instantaneously and cannot be achieved faster while the required work still increases. Hence the process becomes less efficient without any significant gain in time.

The different characteristic times and the required work can be related to the single-particle dynamics already discussed above [18,158]. In a creep experiment, $\langle \Delta y^2(t) \rangle \sim \gamma$ and both increase superlinearly in the transient regime. In contrast, if a step-rate is applied, the MSD also shows transient superdiffusive behaviour but the strain $\gamma(t)$ increases only linearly with time. Thus the dynamics increases faster than the strain $\gamma(t)$ and, therefore, faster than in a creep experiment. This is consistent with the faster yielding and transition to flow observed in step-rate experiments and indicates that the enhanced dynamics are responsible for yielding and flow.

4 Conclusions

We summarized findings on the structure, dynamics and rheological response of glasses formed by binary colloidal mixtures. Special attention was given to the contributions of the authors, namely the link between the macroscopic rheological response and the microscopic structure and dynamics of the individual particles and groups of particles, as obtained by rheology and confocal microscopy, respectively. These findings are put in the context of the work of other groups, providing a comprehensive picture of the behaviour of concentrated colloidal mixtures.

Depending on the size ratio, mixing ratio and total volume fraction, the properties of the concentrated binary mixtures as well as the caging mechanism change. They

form repulsive, attractive and asymmetric glasses as well as gel-like structures and fluids. Binary mixtures thus offer the possibility to investigate and compare different glass states. The state determines the rheological response, but also affects shear-induced changes in the particle structure and dynamics. We focus on the transient responses to the application of a step in shear rate and a step in stress (creep). Shear induces affine motions but also enhances the Brownian motion which facilitates out-of-cage diffusion and leads to the deformation of cages. Under applied stress, the single-particle MSD is approximately linearly related to the macroscopic deformation even in the transient non-linear response regimes, where both increase superlinearly with time if a stress beyond the yield stress is applied. Moreover, also the fraction of active particles as well as active regions, i.e. groups of particles, is proportional to the macroscopic strain. The spatial distribution and evolution of these active regions determines the onset of flow. In contrast, the application of a constant shear-rate implies a linearly increasing strain but causes superdiffusive single-particle dynamics and the deformation and elongation of cages. This results in yielding and the subsequent release of accumulated stresses which causes the stress overshoot. Finally a steady state of flow is reached. In both cases, therefore, the application of shear can induce melting of the glass. The transient response, namely the time and work required to reach yielding and flow, however, depends on the shear protocol. Yielding and flow are achieved faster and more efficiently if a step rate rather than a step stress is applied. This appears to be linked to the faster dynamics in strain-controlled experiments and supports the expectation that yielding and flow are controlled by the dynamics.

Acknowledgements

We thank M. Fuchs, R. Castañeda-Priego, P. Chaudhuri, Th. Franosch, A. Heuer, J. Horbach, G. Petekidis, W. C. K. Poon, K. Samwer, M. Sperl, Th. Voigtmann, E. Zaccarelli and A. Zaccone for many very helpful and inspiring discussions. We gratefully acknowledge funding by the Deutsche Forschungsgemeinschaft (DFG) through the research unit FOR1394, project P2, and funding of the confocal microscope through grant INST 208/6171 FUGG.

References

1. M. Dijkstra, R. van Roij and R. Evans, Phys. Rev. E **59**, 5744 (1999).
2. R. Roth, R. Evans and S. Dietrich, Phys. Rev. E **62**, 5360 (2000).
3. D. J. Ashton, N. B. Wilding, R. Roth and R. Evans, Phys. Rev. E **84**, 061136 (2011).
4. A. D. Dinsmore, A. G. Yodh and D. J. Pine, Phys. Rev. E **52**, 4045 (1995).
5. N. Hunt, R. Jardine and P. Bartlett, Phys. Rev. E **62**, 900 (2000).
6. P. Bartlett, R. H. Ottewill and P. N. Pusey, Phys. Rev. Lett. **68**, 3801 (1992).
7. X. Cottin and P. A. Monson, J. Chem. Phys. **102**, 3354 (1995).
8. A. B. Schofield, Phys. Rev. E **64**, 051403 (2001).
9. A.-P. Hynninen, L. Filion and M. Dijkstra, J. Chem. Phys. **131**, 064902 (2009).
10. R. Seyboldt, D. Hajnal, F. Weysser and M. Fuchs, Soft Matter **8**, 4132 (2012).
11. G. Foffi, W. Götze, F. Sciortino, P. Tartaglia and Th. Voigtmann, Phys. Rev. Lett. **91**, 085701 (2003).
12. R. Juárez-Maldonado and M. Medina-Noyola, Phys. Rev. E **77**, 051503 (2008).
13. A. Imhof and J. K. G. Dhont, Phys. Rev. Lett. **75**, 1662 (1995).
14. A. J. Moreno and J. Colmenero, Phys. Rev. E **74**, 021409 (2006).
15. A. J. Moreno and J. Colmenero, J. Chem. Phys. **125**, 164507 (2006).

16. T. Sentjabrskaja, D. Guu, P. M. Lettinga, S. U. Egelhaaf and M. Laurati, AIP Conf. Proc. **1518**, 206 (2013).
17. T. Sentjabrskaja, E. Babaliari, J. Hendricks, M. Laurati, G. Petekidis and S. U. Egelhaaf, Soft Matter **8**, 4524 (2013).
18. T. Sentjabrskaja, M. Hermes, W. C. K. Poon, C. D. Estrada, R. Castañeda-Priego, S. U. Egelhaaf and M. Laurati, Soft Matter **10**, 6546 (2014).
19. P. Yunker, Z. Zhang and A. G. Yodh, Phys. Rev. Lett. **104**, 015701 (2010).
20. S. Sanyal and A. K. Sood, Phys. Rev. E **57**, 908 (1998).
21. T. Hamanaka and A. Onuki, Phys. Rev. E **75**, 041503 (2007).
22. F. Ebert, P. Keim and G. Maret, Eur. Phys. J. E **26**, 161 (2008).
23. E. Zaccarelli, S. M. Liddle and W. C. K. Poon, Soft Matter **11**, 324 (2015).
24. P. Germain and S. Amokrane, Phys. Rev. Lett. **102**, 058301 (2009).
25. S. R. Williams and W. van Megen, Phys. Rev. E **64**, 041502 (2001).
26. Th. Voigtmann, Europhys. Lett. **96**, 36006 (2011).
27. W. Götze and Th. Voigtmann, Phys. Rev. E **67**, 021502 (2003).
28. P. N. Pusey, in *Liquids, Freezing and Glass Transition* edited by J. P. Hansen, D. Levesque and J. Zinn-Justin (North-Holland, Amsterdam, 1991) p. 763–942.
29. G. L. Hunter and E. R. Weeks, Rep. Prog. Phys. **75**, 066501 (2012).
30. P. N. Pusey and W. van Megen, Phys. Rev. Lett. **59**, 2083 (1987).
31. W. van Megen, T. C. Mortensen, S. R. Williams, and J. Mller, Phys. Rev. E **58**, 6073 (1998).
32. P. N. Pusey and W. van Megen, Nature **320**, 340 (1986).
33. F. Tchangnwa Nya, A. Ayadim, P. Germain and S. Amokrane, J. Phys.: Condens. Matter **24**, 325106 (2012).
34. G. Brambilla, D. El Masri, M. Pierno, L. Berthier, L. Cipelletti, G. Petekidis, and A. B. Schofield, Phys. Rev. Lett. **102**, 085703 (2009).
35. Th. Voigtmann and J. Horbach, Phys. Rev. Lett. **103**, 205901 (2009).
36. E.López-Sánchez, C.D.Estrada-Álvarez,G.Pérez-Ángel, J. M. Méndez-Alcaraz, P. González-Mozuelos and R. Castañeda-Priego, J. Chem. Phys. **139**, 104908 (2013).
37. J. Bosse and J. S. Thakur, Phys. Rev. Lett. **59**, 998 (1987).
38. J. Bosse and Y. Kaneko, Phys. Rev. Lett. **74**, 4023 (1995).
39. L. Sjögren, Phys. Rev. A **33**, 1254 (1986).
40. S. R. Williams, I. K. Snook and W. van Megen, Phys. Rev. E **64**, 021506 (2001).
41. I. Biazzo, F. Caltagirone, G. Parisi and F. Zamponi, Phys. Rev. Lett. **102**, 195701 (2009).
42. R. S. Farr and R. D. Groot, J. Chem. Phys. **131**, 244104 (2009).
43. A. B. Hopkins, F. H. Stillinger and S. Torquato, Phys. Rev. E **85** 021130 (2012).
44. A. B. Hopkins, Y. Jiao, F. H. Stillinger and S. Torquato, Phys. Rev. Lett. **107**, 125501 (2011).
45. R. Kurita and E. R. Weeks, Phys. Rev. E **84**, 030401 (2011).
46. W. Schaertl and H. Sillescu, J. Stat. Phys. **77**, 1007 (1994).
47. V. Baranau and U. Tallarek, Soft Matter **10**, 3826 (2014).
48. P. Charbonneau, A. Ikeda, G. Parisi and F. Zamponi, Phys. Rev. Lett. **107**, 185702 (2011).
49. J. Hendricks, R. Capellmann, A. B. Schofield, S. U. Egelhaaf and M. Laurati, Phys. Rev. E **91**, 032308 (2015).
50. B. E. Rodriguez, E. W. Kaler and M. S. Wolfe, Langmuir **8**, 2382 (1992).
51. R. G. Larson, *The Structure and Rheology of Complex Fluids* (Oxford University Press, 1999).
52. T. G. Mason and D. A. Weitz, Phys. Rev. Lett. **75**, 2770 (1995).
53. A. T. J. M. Woutersen and C. G. de Kruif, J. Rheol. **37**, 681 (1993).
54. P. D'Haene and J. Mewis, Rheol. Acta **33**, 165 (1994).
55. W. Richtering and H. Müller, Langmuir **11**, 3699 (1995).
56. W. J. Hunt and C. F. Zukoski, Langmuir **12**, 6257 (1996).
57. P. Gondret and L. Petit, Langmuir **41**, 1261 (1997).
58. R. Greenwood, P. F. Luckham and T. Gregory, J. Colloid Interface Sci. **191**, 11 (1997).

59. T. Shikata, H. Niwa and Y. Morishima, J. Rheol. **42**, 765 (1998).
60. T. Ohtsuki, Physica A **122**, 212 (1983).
61. G. Nägele and J. Bergenholtz, J. Chem. Phys. **108**, 9893 (1998).
62. R. A. Lionberger, Phys. Rev. E **65**, 061408 (2002).
63. C. Y. Chang and R. L. Powell, J. Fluid Mech. **253**, 1 (1993).
64. C. Y. Chang and R. L. Powell, J. Rheol. **38**, 85 (1994).
65. C. Y. Chang and R. L. Powell, Phys. Fluids **6**, 1628 (1994).
66. R. Foudazi, I. Masalova and A. Y. Malkin, J. Rheol. **56**, 1299 (2012).
67. R. J. Farris, Trans. Soc. Rheol. **12**, 281 (1968).
68. G. Petekidis, A. Moussaid and P. N. Pusey, Phys. Rev. E **66**, 051402 (2002).
69. G. Petekidis, D. Vlassopoulos and P. N. Pusey, Faraday Discuss. **123**, 287 (2003).
70. K. N. Pham, G. Petekidis, D. Vlassopoulos, S. U. Egelhaaf, P. N. Pusey and W. C. K. Poon, Europhys. Lett. **75**, 624 (2006).
71. K. N. Pham, G. Petekidis, D. Vlassopoulos, S. U. Egelhaaf, W. C. K. Poon and P. N. Pusey, J. Rheol. **52**, 649 (2008).
72. R. Besseling, E. R. Weeks, A. B. Schofield, and W. C. K. Poon, Phys. Rev. Lett. **99**, 028301 (2007).
73. N. Koumakis, A. Pamvouxoglou, A. S. Poulos and G. Petekidis, Soft Matter **8**, 4271 (2012).
74. C. Eisenmann, C. Kim, J. Mattsson and D. A. Weitz, Phys. Rev. Lett. **104**, 035502 (2010).
75. M. Siebenbürger, M. Fuchs and M. Ballauff, Soft Matter **8**, 4014 (2012).
76. C. Christopoulou, G. Petekidis, B. Erwin, M. Cloitre and D. Vlassopoulos, Philos. Trans. R. Soc., A **367**, 5051 (2009).
77. K. J. Mutch, M. Laurati, C. P. Amann, M. Fuchs and S. U. Egelhaaf, Eur. Phys. J.: Spec. Top. **222**, 2803 (2013).
78. C. P. Amann, M.Siebenbürger, M.Krüger, F.Weysser, M. Ballauff and M. Fuchs, J. Rheol. **57**, 149 (2013).
79. P. A. Smith, G. Petekidis, S. U. Egelhaaf and W. C. K. Poon, Phys. Rev. E **76**, 041402 (2007).
80. P. Schall, D. A. Weitz and F. Spaepen, Science **318**, 1895 (2007).
81. L. Mohan, C. Pellet, M. Cloitre and R. Bonnecaze, J. Rheol. **57**, 1023 (2013).
82. N. Koumakis, M. Laurati, A. R. Jacob, K. J. Mutch, A. Abdellali, A. B. Schofield, S. U. Egelhaaf, J. F. Brady and G. Petekidis, J. Rheol. **60**, 603 (2016).
83. M. Laurati, P. Maßhoff, K. J. Mutch, S. U. Egelhaaf and A. Zaccone, Phys. Rev. Lett. **118**, 018002 (2017).
84. R. Besseling, L. Isa, E. R. Weeks and W. C. Poon, Adv. Coll. Int. Sci. **146**, 1 (2009).
85. S. K. Dutta, A. Mbi, R. C. Arevalo and D. L. Blair, Rev. Sci. Instrum. **84**, 063702 (2013).
86. M. C. Jenkins and S. U. Egelhaaf, Adv. Colloid Interface Sci. **136**, 65 (2008).
87. W. C. K. Poon, E. R. Weeks and C. P. Royall, Soft Matter **8**, 21 (2012).
88. C. P. Royall, W. C. K. Poon and E. R. Weeks, Soft Matter **9**, 17 (2013).
89. A. Yethiraj and A. van Blaaderen, Nature **421**, 513 (2003).
90. E.-J. Donth, *The Glass Transition: Relaxation Dynamics in Liquids and Disordered Materials* (Springer-Verlag, Berlin Heidelberg, 2001).
91. C. Suryanarayana and A. Inoue, *Bulk Metallic Glasses* (CRC Press, Taylor and Francis Group, 2011).
92. E. R. Weeks, J. C. Crocker, A. C. Levitt, A. Schofield and D. A. Weitz, Science **287**, 627 (2000).
93. W. K. Kegel and A. van Blaaderen, Science **287**, 290 (2000).
94. K. N. Pham, A. M. Puertas, J. Bergenholtz, S. U. Egelhaaf, A. Moussaid, P. N. Pusey, A. B. Schofield, M. Cates, M. Fuchs and W. C. K. Poon, Science **296**, 104 (2002).
95. K. N. Pham, S. U. Egelhaaf, P. N. Pusey and W. C. K. Poon, Phys. Rev. E **69**, 011503 (2004).
96. E. Zaccarelli and W. C. K. Poon, Proc. Natl. Acad. Sci. USA **106**, 15203 (2009).
97. L. J. Kaufman and D.A. Weitz, J. Chem. Phys. **125**, 074716 (2006).

98. T. van de Laar, K. Schroën and J. Sprakel, Sci. Rep. **6**, 22725 (2016).
99. F. Höfling and T. Franosch, Rep. Prog. Phys. **76**, 046602 (2013).
100. H. A. Lorentz, Arch. Neerl. Sci. Exact Natur **10**, 336 (1905).
101. F. Höfling, T. Franosch and E. Frey, Phys. Rev. Lett. **96**, 165901 (2006).
102. T. Sentjabrskaja, E. Zaccarelli, C. De Michele, F. Sciortino, P. Tartaglia, Th. Voigtmann, S. U. Egelhaaf and M. Laurati, Nat. Comm. **7**, 11133 (2016).
103. L. Berthier, G. Biroli, J.-P. Bouchaud, L. Cipelletti and W. van Saarloos, *Dynamical Heterogeneities in Glasses, Colloids, and Granular Media* (Oxford University Press, New York, 2011).
104. W. C. K. Poon, J. Phys.: Condens. Matter **14**, R859 (2002).
105. E. Zaccarelli, J. Phys.: Condens. Matter **19**, 323101 (2007).
106. M. Laurati, G. Petekidis, N. Koumakis, F. Cardinaux, A. B. Schofield, J. M. Brader, M. Fuchs and S. U. Egelhaaf, J. Chem. Phys. **130**, 134907 (2009).
107. M. Laurati, S. U. Egelhaaf and G. Petekidis, J. Rheol. **55**, 673 (2011).
108. N. Koumakis and G. Petekidis, Soft Matter **7**, 2456 (2011).
109. S. A. Shah, Y. L. Chen, S. Ramakrishnan, K. S. Schweizer and C. F. Zukoski, J. Phys.: Condens. Matter **15**, 4751 (2003).
110. P. Varadan and M. J. Solomon, Langmuir **19**, 509 (2003).
111. C. J. Dibble, M. Kogan and M. J. Solomon, Phys. Rev. E **74**, 041403 (2006).
112. M. Kohl, R. F. Capellmann, M. Laurati, S. U. Egelhaaf and M. Schmiedeberg, Nat. Comm **7**, 11817 (2016).
113. R. Pandey and J. C. Conrad, Soft Matter **9**, 10617 (2013).
114. J. M. Lynch, G. C. Cianci and E. R. Weeks, Phys. Rev. E **78**, 031410 (2008).
115. T. Narumi, S. V. Franklin, K. W. Desmond, M. Tokuyama and E. R. Weeks, Soft Matter **7**, 1472 (2011).
116. C. Mayer, E. Zaccarelli, E. Stiakakis, C. N. Likos, F. Sciortino, A. Munam, M. Gauthier, N. Hadjichristidis, H. Iatrou, P. Tartaglia, H. Löwen and D. Vlassopoulos, Nat. Mater. **7**, 780 (2008).
117. C. Mayer, F. Sciortino, C. N. Likos, P. Tartaglia, H. Löwen and E. Zaccarelli, Macromol. **42**, 423 (2009).
118. T. O. E. Skinner, S. K. Schnyder, D. G. A. L. Aarts, J. Horbach and R. P. A. Dullens, Phys. Rev. Lett. **111**, 128301 (2013).
119. R. Higler, J. Appoel and J. Sprakel, Soft Matter **9**, 5372 (2013).
120. N. Koumakis, A. B. Schofield and G. Petekidis, Soft Matter **4**, 2008 (2008).
121. N. Y. C. Lin, S. Goyal, X. Cheng, R. N. Zia, F. A. Escobedo and I. Coehn, Phys. Rev. E **88**, 062309 (2013).
122. M. Ballauff, J. M. Brader, S. U. Egelhaaf, M. Fuchs, J. Horbach, N. Koumakis, M. Krüger, M. Laurati, K. J. Mutch, G. Petekidis, M. Siebenbürger, Th. Voigtmann and J. Zausch, Phys. Rev. Lett. **110**, 215701 (2013).
123. J. Zausch, J. Horbach, M. Laurati, S. U. Egelhaaf, J. M. Brader, Th. Voigtmann and M. Fuchs, J. Phys.: Condens. Matter **20**, 404210 (2008).
124. N. Koumakis, J. F. Brady and G. Petekidis, Phys. Rev. Lett. **110**, 178301 (2013).
125. M. Laurati, K. J. Mutch, N. Koumakis, J. Zausch, C. P. Amann, A. B. Schofield, G. Petekidis, J. F. Brady, J. Horbach, M. Fuchs and S. U. Egelhaaf, J. Phys. Condens. Matter **24**, 464104 (2012).
126. J. Mewis and N. J. Wagner, *Colloidal Suspension Rheology* (Cambridge University Press, New York, 2012).
127. J. S. Harmon, M. D. Demetriou, W. L. Johnson and K. Samwer, Phys. Rev. Lett. **99**, 135502 (2007).
128. K. Osaki, T. Inoue and T. Isomura, J. Polym. Sci. B **38**, 1917 (2000).
129. M. T. Islam and L. A. Archer, J. Polym. Sci. B **39**, 2275 (2001).
130. W. Letwimolnun, B. Vergnes, G. Ausias and P. Carreau, J. Non-Newton. Fluid Mech. **141**, 167 (2007).
131. B. van Aken, P. de Hey and J. Sietsma, Mater. Sci. Eng. A **278**, 247 (2000).
132. W. L. Johnson, J. Lu and M. D. Demetriou, Intermetallics **10**, 1039 (2002).

133. J. M. Brader, Th. Voigtmann, M. Fuchs, R. G. Larson and M. E. Cates, Proc. Natl. Acad. Sci. **106**, 15186 (2009).
134. M. Goldstein, J. Chem. Phys. **51**, 3728 (1969).
135. A. Heuer, J. Phys.: Condens. Matter **20**, 373101 (2008).
136. F. Evers, R. D. L. Hanes, C. Zunke, R. F. Capellmann, J. Bewerunge, C. Dalle-Ferrier, M. C. Jenkins, I. Ladadwa, A. Heuer, R. Castañeda-Priego and S. U. Egelhaaf, Eur. Phys. J. Spec. Top. **222**, 2995 (2013).
137. R. D. L. Hanes, C. Dalle-Ferrier, M. Schmiedeberg, M. C. Jenkins and S. U. Egelhaaf, Soft Matter **8**, 2714 (2012).
138. F. Evers, C. Zunke, R. D. L. Hanes, J. Bewerunge, I. Ladadwa, A. Heuer and S. U. Egelhaaf, Phys. Rev. E **88**, 022125 (2013).
139. C. Dalle-Ferrier, M. Krüger, R. D. L. Hanes, S. Walta, M. C. Jenkins and S. U. Egelhaaf, Soft Matter **7**, 2064 (2011).
140. N. Koumakis, M. Laurati, S. U. Egelhaaf, J. F. Brady and G. Petekidis, Phys. Rev. Lett. **108**, 098303 (2012).
141. X. Cheng, J. H. McCoy, J. N. Israelachvili and I. Cohen, Science **333**, 1276 (2011).
142. F. Varnik, J. Chem. Phys. **125**, 164514 (2006).
143. K. Miyazaki, H. M. Wyss, D. A. Weitz and D. R. Reichman, Europhys. Lett. **75**, 915 (2006).
144. T. Sentjabrskaja, J. Hendricks, A. R. Jacob, G. Petekidis, S. U. Egehaaf and M. Laurati, submitted (2017).
145. P. Oswald, *Rheophysics* (Cambridge University Press, 2009).
146. T. Divoux, C. Barentin and S. Manneville, Soft Matter **7**, 8409 (2011).
147. G. B. McKenna, J. Res. Natl. Inst. Stand. Technol. **99**, 169 (1994).
148. S. M. Fielding, P. Sollich and M. E. Cates, J. Rheol. **44**, 323 (2000).
149. M. L. Falk and J. S. Langer, Phys. Rev. E **57**, 7192 (1998).
150. C. Derec, A. Ajdari and F. Lequeux, Eur. Phys. J. E **4**, 355 (2001).
151. M. Siebenbürger, M. Ballauff and Th. Voigtmann, Phys. Rev. Lett. **108**, 255701 (2012).
152. F. Spaepen, Acta Metall. **25**, 407 (1997).
153. A. S. Argon, Acta Metall. **27**, 47 (1979).
154. W. L. Johnson, M. D. Demetriou, J. S. Hermon, M. L. Lind and K. Samwer, MRS Bull. **32**, 644 (2007).
155. E. N. Andrade, Proc. R. Soc. Lond. A **84**, 1 (1910).
156. P. Chaudhuri and J. Horbach, Phys. Rev. E **88**, 040301 (2013).
157. J. Rosti, J. Koivisto, L. Laurson and M. Alava, Phys. Rev. Lett. **105**, 100601 (2010).
158. T. Sentjabrskaja, P. Chaudhuri, M. Hermes, W. C. K. Poon, J. Horbach, S. U. Egelhaaf and M. Laurati, Sci. Rep. **5**, 11884 (2015).
159. P. Ballesta and G. Petekidis, Phys. Rev. E **93**, 042613 (2016).
160. P. Coussot, H. Tabuteau, X. Chateau, L. Tocquer and G. Ovarlez, J. Rheol. **50**, 975 (2006).
161. K. Chen, K. S. Schweizer, R. Stamm, E. Lee and J. M. Caruthers, J. Chem. Phys. **129**, 184094 (2008).
162. K. Chen and K. S. Schweizer, Phys. Rev. E **82**, 041804 (2010).
163. K. Chen, E. J. Saltzmann and K. S. Schweizer, Annu. Rev. Condens. Matter Phys. **1**, 277 (2010).
164. A. Amon, V. B. Nguyen, A. Bruand, J. Crassous and E. Clement, Phys. Rev. Lett. **108**, 135502 (2012).
165. L. Bocquet, A. Colin and A. Ajdari, Phys. Rev. Lett. **103**, 036001 (2009).
166. V. Chikkadi, G. Wegdam, D. Bonn, B. Nienhuis and P. Schall, Phys. Rev. Lett. **107**, 198303 (2011).
167. A. Lemaitre and C. Caroli, Phys. Rev. Lett. **103**, 065501 (2009).
168. S. Karmakar, E. Lerner and I. Procaccia, Phys. Rev. E **82**, 055103 (2010).
169. J.-O. Krisponeit, S. Pitikaris, K. E. Avila, S. Küchelmann, A. Krüger and K. Samwer, Nat. Comm. **5**, 3616 (2014).
170. C. Herrero-Gómez and K. Samwer, Sci. Rep. **6**, 33503 (2016).
171. H. G. E. Hentschel, M. Moshe, I. Procaccia and K. Samwer, Philos. Mag. **96**, 1399 (2016).